J. Fluid Mech. (2013), *vol.* 737, *pp.* 308–328.
doi:10.1017/jfm.2013.563

Nematic–isotropic phase transition in turbulent thermal convection

Stephan Weiss and Guenter Ahlers†

[1]Department of Physics, University of California, Santa Barbara, CA 93106, USA

(Received 31 July 2013; revised 31 July 2013; accepted 20 October 2013;
first published online 25 November 2013)

We report on turbulent Rayleigh–Bénard convection of a nematic liquid crystal while it undergoes a transition from the nematic to the isotropic phase in a cylindrical convection cell with a height equal to twice the diameter (aspect ratio $\Gamma = 0.50$). The difference between the top and bottom plate temperature $\Delta T = T_b - T_t$ was held constant, while the average temperature $T_m = (T_b + T_t)/2$ was varied. There was a significant increase of the transported heat when the phase transition temperature T_{NI} was between T_b and T_t. Measurements of the temperatures along the sidewall of the sample as a function of T_m showed several ranges with qualitatively different behaviour of quantities such as the time-averaged sidewall temperature, temperature gradient, or temperature fluctuations. We interpret these different ranges in terms of properties of the thermal boundary layers close to the top and bottom plates whose stability and nature depends on the location within the sample of T_{NI}.

Key words: Bénard convection, drops and bubbles, moist convection

1. Introduction

Thermal convection is the fluid motion driven by a thermal gradient in the presence of gravity; for reviews, see Kadanoff (2001), Ahlers (2009), Ahlers, Grossmann & Lohse (2009), Lohse & Xia (2010) and Chillà & Schumacher (2012). It is a very effective heat-transport mechanism and therefore important in many natural systems (Marshall & Schott 1999; Rahmstorf 2000; Hartmann, Moy & Fu 2001), for industrial applications (Brent, Voller & Reid 1988; Kühn, Bosbach & Wagner 2009; Iezzi, Francolino & Mucchetti 2011), as well as in daily life. To study thermal convection in controlled experiments or to investigate it numerically, simplified systems are considered in which a simple fluid (Newtonian and isotropic) is confined between two parallel horizontal plates. While the top plate is cooled, the bottom plate is heated. For temperature differences $\Delta T = T_b - T_t$ between the two plates that are not too large, the fluid properties can be assumed to be constant (the Oberbeck–Boussinesq or OB approximation: Oberbeck 1879; Boussinesq 1903) and the system is governed by only two dimensionless parameters. These are the Rayleigh number

$$Ra = \frac{g\alpha \Delta T L^3}{\nu\kappa}, \tag{1.1}$$

† Email address for correspondence: guenter@physics.ucsb.edu

and the Prandtl number

$$Pr = \nu/\kappa. \tag{1.2}$$

Here L is the distance between the two plates, g is the gravitational acceleration, α is the isobaric thermal expansion coefficient, ν is the kinematic viscosity, and κ is the thermal diffusivity of the fluid. The Rayleigh number is the dimensionless form of the temperature difference and is thus the parameter that can be easily controlled in an experiment, while Pr depends only on the fluid properties and usually does not vary much in a given experiment. Besides these two parameters, only the nature of the boundaries can influence the fluid flow and thus the heat transport. Most experimental and numerical studies used or assumed a cylindrical container of diameter D, which introduced the aspect ratio $\Gamma \equiv D/L$ as a third parameter.

In most of the experimental investigations of thermal convection, simple fluids with nearly constant physical properties were used. In natural systems, however, fluid properties often depend on the temperature, and in interesting cases the fluid even undergoes a first-order phase transition. When a phase transition takes place, bubbles of the low-density phase or drops of the high-density phase can form in the convecting system. Due to the latent heat of vaporization, their transport can contribute importantly, and under appropriate conditions even overwhelmingly, to the heat transport.

One can roughly distinguish two types of phase transitions that play a role in turbulent convection. The first occurs when the two phases have very different physical properties (e.g. the mass density) and when the latent heat of the transition is large and thus contributes in a major way to the heat transport (see, for instance, Zhong, Funfschilling & Ahlers 2009). For example, at a typical liquid–vapour transition such as water at its normal boiling point, the latent heat is of order 2000 kJ kg^{-1} and the densities of the two phases differ by orders of magnitude. The heat transport can then be much larger, by an order of magnitude or more, than it is for single-phase convection at similar Ra. This case is important in many physical situations such as during cloud formation (see, for instance, Auernhammer, Vollmer & Vollmer 2005; Stevens 2005; Weidauer, Pauluis & Schumacher 2010; Pauluis & Schumacher 2011), as well as in numerous engineering applications when heat has to be transported effectively (see, for instance, Zerban & Nye 1956; Tong & Tang 1997; Dhir 1998).

The second type concerns systems where the fluid undergoes a *soft* phase change, meaning the physical properties of both phases are very similar and the latent heat and density discontinuity at the transition are small. This is the case of interest for the present paper. For the fluid used in the present study the latent heat was only 1.56 kJ kg^{-1} (Thoen 1992; van Roie *et al.* 2005), i.e. three orders of magnitude less than the previous example, and the density changed by only 0.2 %. Important examples of soft phase transitions occurring in nature involve convection in the Earth's mantle (see, for instance, Verhoogen 1965; Kerr 1992; Christensen 1995; Shim, Duffy & Shen 2001) where the mantle material is subject to several phase changes. For these transitions only the crystalline structure changes, and thus properties such as the density or the heat conductivity change by only a few per cent. While the transported heat is smaller for these systems, the effect on the flow structure can be significant and thus has been the subject of investigations for several decades: see, for instance, Verhoogen (1965), Kerr (1992), Weinstein (1993), Christensen (1995) and Jacobs & van den Berg (2011).

Already for the case of relatively small Rayleigh numbers unexpected effects can occur in systems with soft phase changes. Using linear stability analysis, Busse &

System	$\Delta\rho/\rho$	ΔH (kJ kg^{-1})	Range of Ra	Pr
5CB	0.002	1.57	3×10^7–6×10^8	400
Mantle transitions	0.02–0.09	0.4–1.2	$O(10^7)$	Nearly ∞

TABLE 1. Comparison of typical parameters for the nematic–isotropic transition in 5CB (Thoen 1992; Ahlers 1995; van Roie *et al.* 2005) and for phase transitions in the Earth's mantle (see, for instance, Verhoogen 1965; Christensen 1995).

Schubert (1971) found that a denser phase on top of the less dense one can be stable, while the opposite can be unstable. These results were confirmed and extended experimentally and theoretically by Ahlers, Berge & Cannell (1993) and Sakurai *et al.* (1999) (see also Ahlers 1995). Those authors investigated the onset of convection in a thin layer of the liquid crystal 5CB (see § 2.2 below) while the top plate was colder and the bottom plate warmer than the transition temperature at which the liquid turns from the nematic phase into the isotropic one. It was found that, depending on the average temperature T_m, the quiescent fluid layer can be stable in a certain range of ΔT, while for both smaller and larger ΔT the fluid becomes unstable and convection sets in.

While the theoretical and experimental work at small Ra near the onset of convection in systems with soft phase transitions had yielded significant insight, the Ra range typical of mantle convection heretofore, so far as we know, had been studied primarily by obtaining solutions of model equations using numerical methods (see, for instance, Schubert 1992; Christensen 1995). The work we report on here is, we believe, the first experimental study at very large Pr and for $Ra \simeq 10^8$ or so which is typical of mantle convection. Thus it is worthwhile comparing some of the relevant parameters that are involved in these two cases: they are collected in table 1. One sees that the mantle transitions involve a larger (albeit still small) density discontinuity, but about the same latent heat ΔH. The range of the Rayleigh number of the experiment is comparable to that found in the mantle. Although the mantle Prandtl number is effectively infinite and the experimental value is finite, we note that many features of turbulent convection do not change much as Pr increases from the experimental value of $\sim$400 to much larger values. Of course there remain major differences between the experimental system and mantle convection. Important ones are that in the geophysical system there is internal heating as well as heating from below, that the mantle is laterally extended and curved while our sample was confined by sidewalls, that non-OB effects are unimportant in the experiment but play a major role in the physical system, and that the latent heat in the mantle transitions can be positive or negative depending on which transition is of interest, as well as many others. Nonetheless, the present study comes closer to the physical system than any other experiment known to us.

In this paper we report on thermal convection at *large* Rayleigh numbers where the fluid is nearly turbulent. We use a nematic liquid crystal (NLC) as the working fluid and investigate the convective heat transport while the NLC undergoes a transition from the nematic to the isotropic phase. NLCs are fluids that consist of elongated or discoidal molecules that, due to their steric interactions, align their preferred axes parallel to each other; see, for instance, de Gennes & Prost (1995) and Khoo (2007). The *director* field $\hat{n}$ represents the direction of the preferred

molecular alignment, averaged over a mesoscopically small region, as a function of the spatial coordinates. While still having Newtonian shear properties, NLCs show a broken rotational symmetry and a spatial order on intermediate length scales ($O(\mu m)$). However, the interaction leading to alignment is rather weak and at a certain temperature the molecules lose their alignment and the fluid turns into an isotropic fluid. The temperature T_{NI} at which the transition occurs is called the *clearing point* because the fluid is opaque below and transparent above T_{NI}. For many NLCs T_{NI} is close to room temperature. The transition at T_{NI} is weakly first-order for many NLCs, i.e. various physical properties show discontinuities at T_{NI}, but these discontinuities, as well as the associated latent heat, are small.

The correlation length over which the director of the NLC is ordered ($O(\mu m)$) is several orders of magnitude shorter than the characteristic dimensions of the sample ($O(10\ cm)$). Therefore, the vigorous fluctuations of the velocity field at large Ra produce a homogeneous distribution of the director throughout the sample. As a result, the convective heat transport by the NLC is similar to that of an isotropic fluid, as long as no external magnetic field is applied (Weiss & Ahlers 2013). A magnetic field aligns the director in thermal and viscous boundary layers adjacent to the top and bottom plates. Thus the heat transport was enhanced by the field because the conductivity of the NLC is larger in a direction parallel to $\hat{n}$ than it is in the perpendicular direction. Experimental data presented here were all taken without an external field and therefore we can neglect the anisotropic nature of the nematic phase in the following.

The remainder of this paper is organized as follows. In the next section, we briefly describe the experimental apparatus, the measurement procedure, and the properties of the fluid. In § 3 we present the measurements and discuss possible explanations of the results. We end the paper with a brief conclusion in § 4.

2. Experimental setup and fluid properties

2.1. *Experimental setup and procedure*

The experiments were carried out in the 'small convection apparatus' (SCA) that was used previously to investigate the influence of a magnetic field on turbulent convection of a liquid crystal (Weiss & Ahlers 2013). The apparatus was described in more detail by Weiss & Ahlers (2011). The cylindrical convection cell consisted of a Lexan sidewall with an inner diameter $D = 95.3$ mm, a wall thickness of 3.2 mm, and a length $L = 190.5$ mm. It was closed by two copper plates, one each at the top and bottom, resulting in a cell with aspect ratio $\Gamma = 0.500$. The cylinder was levelled within 10^{-4} rad. While the top plate was temperature-controlled by a circulating water bath, the bottom plate was heated by a metal-film heater (90 Ω) glued to its underside. Two thermistors, previously calibrated against a standard platinum thermometer, were installed in each of the plates for temperature measurements, and computer-controlled feedback loops kept both plates at the desired temperature during an experimental run.

The convection cell was located in an air and foam filled inner container which itself was surrounded by the temperature-controlled cooling water at temperature T_t which was used to control the top plate temperature. The foam minimized heat loss from the cell to the cooling bath (see figure 1 of Weiss & Ahlers 2011). Prior to the convection experiments we measured the heat conductivity of the 'empty' cell (i.e. a cell filled with foam in order to suppress convection of the air). These measurements thus took into account both the heat transfer along the sidewall and the heat loss of the cell to its surroundings which was at T_t.

Twenty-four thermistors were installed in the sidewall. They were arranged in three sets, each set containing eight thermometers equally spaced azimuthally in a horizontal circle. The three sets were located at vertical positions $z = L/4$, $L/2$ and $3L/4$ away from the bottom plate. We shall use the notation $T_{k,i}$ to identify these thermometers. Here $k = b, m,$ or t, where b, m, t stand for the 'bottom', 'middle', and 'top' set. The index i identifies thermometers 1 to 8 in a given set. In the figures below in § 3.2 we shall use red, green, or blue symbols to represent data for the bottom, middle, or top set respectively. Also below, in § 3.2, we shall examine the three average temperatures

$$T_{w,k} = \frac{1}{8}\sum_{i=1}^{8} \tilde{T}_{k,i}, \tag{2.1}$$

where

$$\tilde{T}_{k,i} = \langle T_{k,i}(t)\rangle_t, \tag{2.2}$$

as well as the three root mean square deviations

$$\sigma_k = \frac{1}{8}\sum_{i=1}^{8} \sqrt{\langle (T_{k,i}(t) - \tilde{T}_{k,i})^2\rangle_t}. \tag{2.3}$$

Here $\langle\cdots\rangle_t$ indicates the time average.

As described elsewhere (Brown, Nikolaenko & Ahlers 2005; Funfschilling, Brown & Ahlers 2008), all sidewall thermistors were immersed in blind holes entering the sidewall from the outside. Thus, the thermistors were not in actual contact with the fluid. While this technique gave excellent sidewall temperature readings in apparatus where a side shield was present that was set at the mean temperature $T_m \equiv (T_b + T_t)/2$, in our case the sidewall was surrounded by the can at temperature $T_t = T_m - \Delta T/2$. Thus, there was a small parasitic heat current from the sidewall to the can. This led to a small temperature offset of the measured sidewall temperatures. For $\Delta T = 6$ K this offset was approximately 0.84 K, although it is not known precisely. For the data shown below we added 0.84 K to the actual measurements. This caused $T_{w,k}$ in the single-phase regions all to be not very far from T_m, as they should be for a near-Boussinesq system. The experimental temperature offset is expected to have no significant influence on the dependence of $T_{w,k}$ on T_m in the two-phase region and on the small temperature variation $T_{w,b} - T_{w,t}$ vertically along the sidewall. It is likely that the fluctuation sizes σ_k are reduced below their actual values in the fluid, but the dependence of σ_k on T_m nonetheless gives useful information, as we shall see in § 3.2.

All thermistors as well as the heat input to the bottom plate were measured every 3.2 s for the duration of an experimental run at a given ΔT and T_m (a day or so). During a typical experimental run, ΔT and T_m were kept constant while measurements were taken for ∼24 h. Then T_m was changed while ΔT was held constant and measurements were taken for the next 24 h, and so on. We report results for $\Delta T = 1$, 2 and 6 K and a variety of different T_m covering the transition region, i.e. the T_m region where the convective fluid undergoes the phase transition.

2.2. *Fluid properties*

We used the nematic liquid crystal 4-Cyano-4′-pentylbiphenyl (5CB) as the convecting fluid. It was chosen because it is not excessively toxic, because it has a convenient clearing point close to room temperature ($T_{NI} = 35.17$ °C), because its cost (although still high) is manageable, and because its physical properties are fairly well known and,

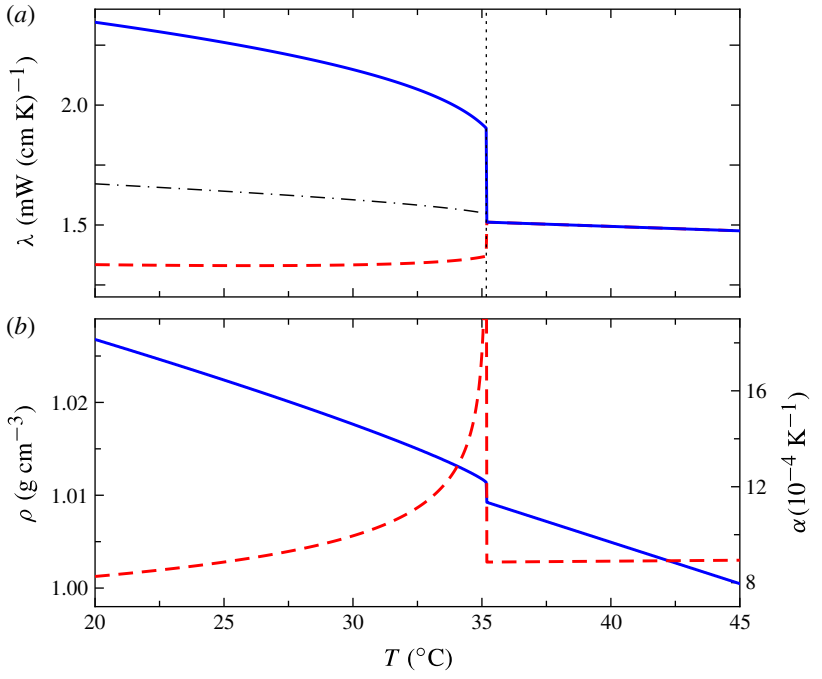

FIGURE 1. (Colour online) Properties of 5CB as a function of temperature. (*a*) Heat conductivity parallel to the director alignment $\hat{n}$ ($\lambda_\parallel$, solid line, blue online), perpendicular to it ($\lambda_\perp$, dashed, red online), and the averaged conductivity relevant to random orientations of $\hat{n}$ ($(\lambda_\parallel + 2\lambda_\perp)/3$, dot-dashed, black). The vertical dotted line marks the clearing point at 35.17 °C. (*b*) Density (solid, blue online, left *y*-axis) and volume expansion coefficient (dashed, red online, right *y*-axis) as a function of temperature. Both plots are based on experimental data and their fitted functions published by Ahlers *et al.* (1994) and Ahlers (1995).

based on a survey of the literature, have been conveniently compiled (Ahlers 1995). Of this material 2.5 kg were obtained from Tokyo Chemical Industry America (TCI) for this experiment and that of Weiss & Ahlers (2013) at a cost of approximately USD 6000.

From the anisotropic fluid properties, only the thermal conductivity λ and the thermal diffusivity $\kappa = \lambda/c_p\varrho$ are relevant in thermal convection (see (1.1) and (1.2)). Both quantities depend on the orientation of the director. Figure 1(*a*) shows the conductivity in the direction parallel to $\hat{n}$ ($\lambda_\parallel$, solid line, blue online) and perpendicular to it ($\lambda_\perp$, dashed line, red online). For $T < T_{NI}$, the difference between $\lambda_\parallel$ and $\lambda_\perp$ becomes smaller as the temperature T increases. Above T_{NI}, the anisotropy disappears and only one value exists for the heat conductivity – the fluid turns into an isotropic liquid. For a sample of rod-like molecules like 5CB we expect that the measured conductivity of a sample with random director orientation (on macroscopic length scales) will be given by

$$\lambda_{avg} = (\lambda_\parallel + 2\lambda_\perp)/3. \tag{2.4}$$

As can be seen from figure 1(*a*), $\lambda_\parallel$ varies significantly with temperature, and both $\lambda_\perp$ and $\lambda_\parallel$ have significant discontinuities at T_{NI}. However, λ_{avg} varies only a little with T and its discontinuity at T_{NI} is very small. Thus, the Nusselt number, which we take to

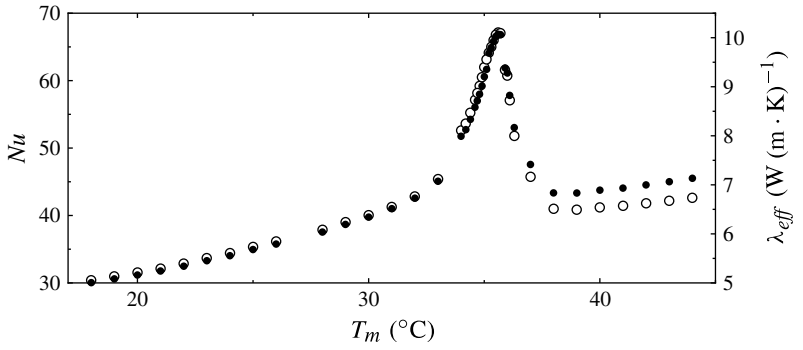

FIGURE 2. The effective thermal conductivity λ_{eff} (open circles, right y-axis) and the Nusselt number Nu (solid circles, left y-axis) as a function of the mean temperature T_m. The measurements were made with $\Delta T = 6$ K. The scales of the vertical axes were chosen so as to cause λ_{eff} and Nu to nearly coincide below T_{NI}.

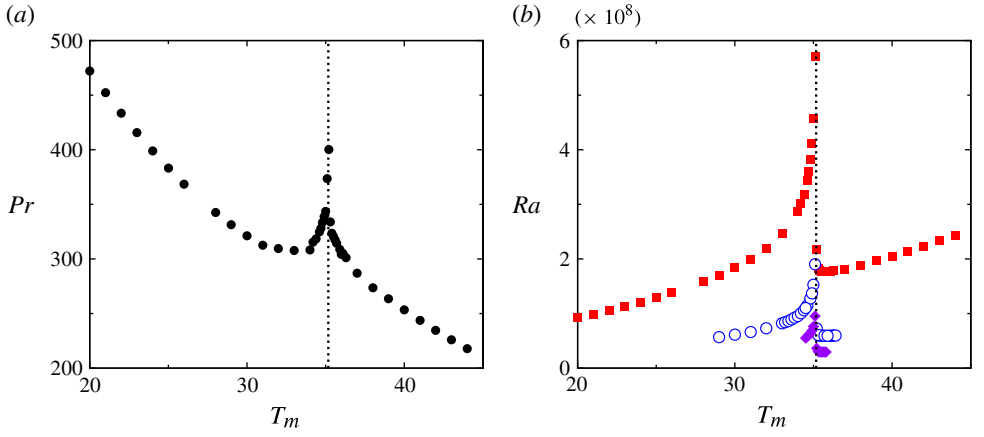

FIGURE 3. (Colour online) (*a*) Prandtl number of 5CB as a function of the temperature. (*b*) Rayleigh number as a function of T_m for $\Delta T = 6$ K (squares, red online), $\Delta T = 2$ K (open circles, blue online) and $\Delta T = 1$ K (diamonds, purple online). The calculations of Ra and Pr are based on the fluid properties at T_m, a heat conductivity $\lambda = (2\lambda_\perp + \lambda_\parallel)/3$, and a clearing point $T_{NI} = 35.17$ °C (vertical dotted lines in (*a*,*b*)).

be given by

$$Nu \equiv \lambda_{eff}/\lambda_{avg} \tag{2.5}$$

with

$$\lambda_{eff} = \frac{QL}{A\Delta T} \tag{2.6}$$

(Q is the heat current and A the cross-sectional area of the cell), is not directly influenced very much by non-OB effects, although of course the strong temperature dependence for instance of Ra (see figure 3*b* below) may have an indirect influence.

We compare results for λ_{eff} with those for Nu in figure 2. They are seen to have a very similar dependence on T_m. Nonetheless we shall report further results in terms of

Properties	ϱ (g cm^{-3})	α (1 K^{-1})	λ (W cm^{-1} K)	κ (cm^2 s^{-1})	Ra/Δ T	Pr
Nematic phase ($T = 32$ °C)	1.0155	11.0×10^{-4}	1.59×10^{-3}	8.042×10^{-4}	2.9×10^{8}	309.5
Isotropic phase ($T = 38$ °C)	1.0067	8.9×10^{-4}	1.52×10^{-3}	8.370×10^{-4}	2.5×10^{8}	273.6

TABLE 2. Typical values for fluid properties in the nematic and the isotropic phase. Adapted from Ahlers (1995) and references therein.

λ_{eff} because the meaning of Nu is ambiguous in the two-phase region, where some of the sample is in one phase while T_m is in the other.

As T varies and then passes through the transition, the mass density changes as well. However, as shown in figure 1(*b*), the density changes only very slightly with temperature below and above T_{ni}, and the density discontinuity at T_{ni} is only $\sim$0.2 % (see Ahlers 1995). This small density drop is in contrast to typical convection systems with liquid–gas phase transitions, where the density drops by a factor of 1000 or even more. Interestingly, it is, however, comparable to the density discontinuities expected at certain depths in the Earth's mantle; see, for instance, Verhoogen (1965), Kerr (1992) and Christensen (1995). As discussed in § 1, we call such a transition with a small density discontinuity and an associated small latent heat a *soft phase transition*. We also show in figure 1(*b*) the volume expansion coefficient α as a function of the temperature. While α is nearly constant for temperature $T > T_{ni}$, it increases significantly with temperature below T_{ni}. However, α remains fairly small and – for temperatures not too close to T_{ni} – is of the order of $10^{-3}/\mathrm{K}^{-1}$. That means that the density difference (and thus the buoyancy) between the nematic and the isotropic phase is similar to that of two volumes of the same phase that differ in temperature by $\sim$2 K.

The exact value of T_{NI} can vary somewhat, perhaps due to differing (albeit small) amounts of impurities. While Ahlers *et al.* (1994) (see also Ahlers 1995 and van Roie *et al.* 2005) measured $T_{NI} = 35.17$ and 35.2 °C respectively, Bezrodna *et al.* (2008) found a higher value of 35.55 °C. Thus we re-determined T_{NI}, using the sample of the present work. For this purpose a small amount of the NLC was placed in a glass tube, and the tube was inserted in a temperature-controlled water bath. The clearing point could easily be identified visually. We found that it shifted slightly during our experiment. For a fresh sample of 5CB we measured $T_{NI} = 35.20 \pm 0.03$ °C, while we measured a slightly lower $T_{NI} = 35.07 \pm 0.04$ °C for 5CB after it had been used in our experiment for a couple of months. The value cited by Ahlers (1995) is not far from (and indeed between) these values. Since we based our data analysis on the fluid properties compiled by Ahlers (1995), we used 35.17 °C in further data analysis.

For a nematic liquid crystal there are five independent viscosities which can be expressed in terms of the Leslie coefficients α_i (see, for instance, de Gennes & Prost 1995). The equivalent of the kinematic viscosity of an isotropic fluid is given by $\nu = \alpha_4/2\rho$. This parameter is used to determine Ra and Pr using (1.1) and (1.2) (see, for instance, Kramer & Pesch 1995). As an overview we present in table 2 typical values for the fluid properties of the nematic phase (at $T = 32$ °C) and of the isotropic phase (at $T = 38$ °C).

Figure 3 shows how the changes with temperature of fluid properties affect Pr and Ra. The calculation of these parameters assumed constant properties throughout the

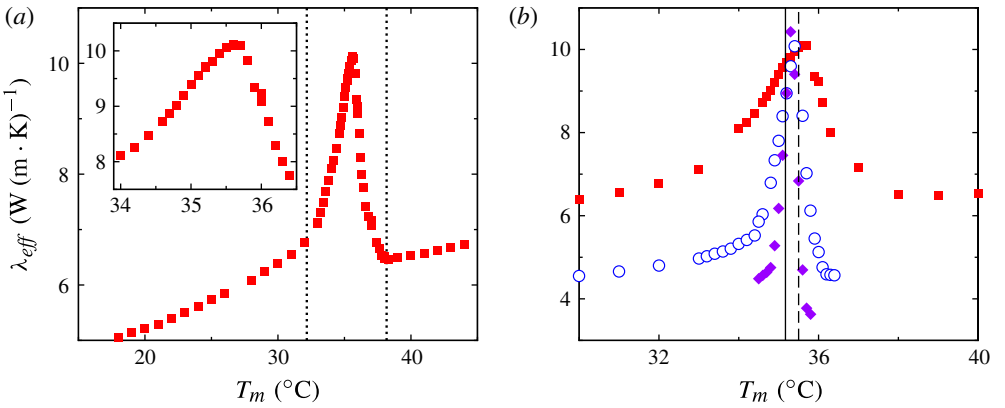

FIGURE 4. (Colour online) The effective heat conductivity λ_{eff} as a function of the mean temperature T_m. (*a*) Data for $\Delta T = 6$ K covering a large range of T_m. The inset shows the region close to the maximum. The area between the two vertical dotted lines represents the temperature range between T_b and T_t over which we expect the phase transition to occur, i.e. where T_{NI} occurs somewhere in the sample. (*b*) Data for $\Delta T = 6$ K (squares, red online), $\Delta T = 2$ K (open circles, blue online), and $\Delta T = 1$ K (diamonds, purple online) over a narrower temperature range. The black solid (dashed) vertical line marks T_{NI} as given by Ahlers *et al.* (1994) (Bezrodna *et al.* 2008).

cell. Away from T_{NI}, Pr decreases and Ra increases with increasing temperature, while for both a sharp peak appears right at T_{NI}. The maximum of Ra at $T_{NI} \approx 35.17$ °C is about three times larger than Ra at $T_m = 36$ °C, for instance. This strong temperature dependence is due primarily to that of the expansion coefficient α (see (1.1)). Thus, near the transition the OB approximation is not very good. It is, however, well established that results for $Nu(Ra)$ in a single-phase fluid are not influenced strongly by deviations from the OB approximation of the type encountered here (Ahlers *et al.* 2006, 2007, 2008). Further away from T_{NI}, deviations from the OB approximation rapidly decrease as $|T_m - T_{NI}|$ increases.

We shall present our results mostly as a function of T_m. Nonetheless, we have to recall the results for Ra in figure 3 in the next section, when we analyse the heat transport with the phase transition present in order to distinguish between contributions from the phase transition itself and contributions due to changes of the fluid properties.

3. Results

3.1. *Heat transport*

Figure 4(*a*) shows λ_{eff} as a function of T_m for an applied temperature difference $\Delta T = 6$ K. The region between the vertical dotted lines marks the range where both phases are expected to co-exist. To the left of it, in the nematic phase, λ_{eff} increases monotonically with T_m. For T_m between 32.2 and 38.2 °C, the fluid constantly changes from one phase to the other while it convects from the top to the bottom plate and back. In analogy to a liquid–gas phase transition, we will refer to the formation of the high (low) temperature isotropic (nematic) phase at the bottom (top) plate of the cell as 'bubble' ('droplet') formation, even though in this case the difference in density between the bubbles and droplets is very small. In this two-phase range the increase of λ_{eff} with T_m first becomes steeper and then decreases after passing through a maximum

near $T_m \approx 35.5$ °C. Beyond $T_m \approx 38.2$ °C the sample is entirely in the isotropic phase where λ_{eff} gradually increases.

It is apparent that the region with the most rapid increase and decrease of λ_{eff} is where a phase transition is expected to be present and thus where latent heat effects may contribute. The more gradual increase of λ_{eff} with T_m in the single-phase regions is due to an increase of Ra (see figure 3), which is caused by the change of fluid properties as T_m changes.

The maximum of λ_{eff} in the two-phase region is not symmetric about T_m (see inset of figure 4*a*). Close to the maximum the slope of the curve becomes smaller and reaches a small plateau at $T_m \approx 35.7$ °C. For slightly larger T_m, there is a small discontinuous drop of λ_{eff}. The decrease beyond the discontinuity is steeper than the increase below the maximum. We investigated whether the asymmetry is associated with hysteresis, but could not find such an effect. At least part of this asymmetry comes from the asymmetric peak of $Ra(T)$ (and thus of $Nu(T)$) displayed in figure 3(*b*) (see also the asymmetric peak of λ_{exp} shown below in figure 5*a*). We can not say whether there is a contribution to the asymmetry from the latent heat released due to the two-phase nature of the system.

Figure 4(*b*) shows some of the same data as figure 4(*a*) on an expanded horizontal scale, and also includes results for $\Delta T = 2$ K (open circles, blue online) and $\Delta T = 1$ K (diamonds, purple online). It is expected that, far away from T_{NI}, λ_{eff} is largest for $\Delta T = 6$ K and smallest for $\Delta T = 1$ K because Ra, and thus also Nu, increases with ΔT. For each of these measurements, the maximum is located close to (but not necessarily at) $T_m \approx T_{NI}$ as expected. The maximum value of λ_{eff} is nearly independent of ΔT. However, the maximum heat current, proportional to $\lambda_{eff}\Delta T$, is largest for the largest ΔT.

For a further discussion of the two-phase region it is useful to define the temperature fraction

$$\phi = 0.5 + (T_m - T_{NI})/\Delta T. \tag{3.1}$$

Then the potential two-phase region can exist over the range $0 \leqslant \phi \leqslant 1$. We are not aware of a way to accurately separate the contribution to λ_{eff} for $0 \leqslant \phi \leqslant 1$ into contributions from latent-heat and density-discontinuity effects on the one hand and from single-phase turbulent convection on the other. Nonetheless, we can make an estimate

$$\lambda_{trans} \equiv \lambda_{eff} - \lambda_{exp} \tag{3.2}$$

of the part that is to be attributed to the phase transition. Here $\lambda_{exp}(T_m)$ is the expected conductivity of the single-phase turbulent system at a temperature $T = T_m$. To estimate $\lambda_{exp}(T_m)$, we first compute $Ra(T_m)$ and $Pr(T_m)$ (equations (1.1) and (1.2)) using the fluid properties at T_m. An example is given in figure 3. We then obtain the single-phase value of $Nu(Ra, Pr)$ (and thus λ_{exp}, see (2.5)) from a fit of our single-phase measurements, both above and below T_{NI}, to the power law $Nu = Nu_0 Pr^{\alpha} Ra^{\gamma}$. This estimate should be valid in the limit as $\Delta T \to 0$, but for finite ΔT we expect the true λ_{exp} (which is unknown to us at the quantitative level) to be more rounded over the interval spanned by ΔT. An example of λ_{exp} for $\Delta T = 6$ K is shown as open squares in figure 5(*a*). One sees that there is fairly good agreement with the measured λ_{eff} in the single-phase regions. However, in the two-phase region (between the two vertical lines) λ_{exp} is smaller than λ_{eff}, indicating that there is an additional contribution λ_{trans} from the phase transition to λ_{eff}. In the absence of effects from the latent heat and the density discontinuity we would have expected λ_{eff} in the two-phase region to be

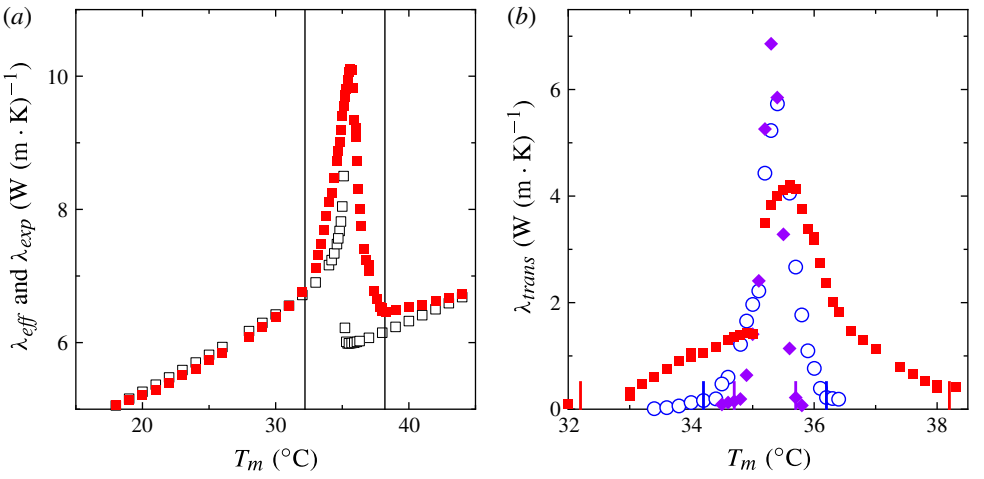

FIGURE 5. (Colour online) (*a*) The effective heat conductivity λ_{eff} (squares, red online), and the expected effective heat conductivity λ_{exp} without a phase transition (open squares), both for $\Delta T = 6$ K and as a function of the average temperature T_m. The two vertical lines indicate the boundaries of the two-phase region in the physical system (i.e. $\phi = 0$ and 1). (*b*) The part $\lambda_{trans} = \lambda_{eff} - \lambda_{exp}$ of the effective heat conductivity that is attributed to the phase transition from the nematic to the isotropic phase. Data are for $\Delta T = 1$ K (solid diamonds, purple online), $\Delta T = 2$ K (open circles, blue online) and $\Delta T = 6$ K (solid squares, red online). The short vertical lines near the bottom horizontal axis give the values of T_m where the top or bottom plate temperature reaches T_{NI}.

smaller than λ_{exp} because at most one of the boundary layers (which control the heat transport) can be near the maximum of λ_{exp}. Results for λ_{trans} for all three values of ΔT are given in figure 5(*b*).

An interesting feature revealed in figure 5(*b*) (at least for the larger ΔT) is a shift, relative to T_{NI}, of the temperature $T_{b,on}$ for the start of the formation of the isotropic phase at the hot (bottom) plate. This is illustrated by the small vertical lines in figure 5(*b*), which give T_m when the top (cold) and bottom (warm) plates have reached the bulk transition temperature T_{NI}. As T_m increases from the nematic phase into the two-phase region, the data suggest that the increase of λ_{trans} above zero at $T_{b,on}$ does not happen until $T_{b,on}$ exceeds T_{NI} by five per cent or so of ΔT. The analogous phenomenon does not seem to occur noticeably at the top plate, where with decreasing T_m the first droplet formation of the nematic phase occurs when $T_{t,on} \simeq T_{NI}$ within the resolution of the data. Closely related phenomena will be discussed in § 3.2.2 below. We note that a shift similar to that of $T_{b,on}$ relative to T_{NI} was observed by Zhong *et al.* (2009) near a liquid–gas phase transition. In their case, however, $T_{t,on}$ was shifted below the phase transition temperature, i.e. there was a delay of the formation of liquid droplets near the top plate as T_m was decreased.

3.2. *Sidewall temperature distribution*

Here we shall discuss the measurements of the sidewall temperatures with the three sets of eight thermometers each discussed in § 2.1. We did not find any evidence for a large-scale circulation, and report here only on the three azimuthally and temporally averaged temperatures $T_{w,k}$ of the eight temperatures $T_{k,i}$ at each level $k = b, m, t$

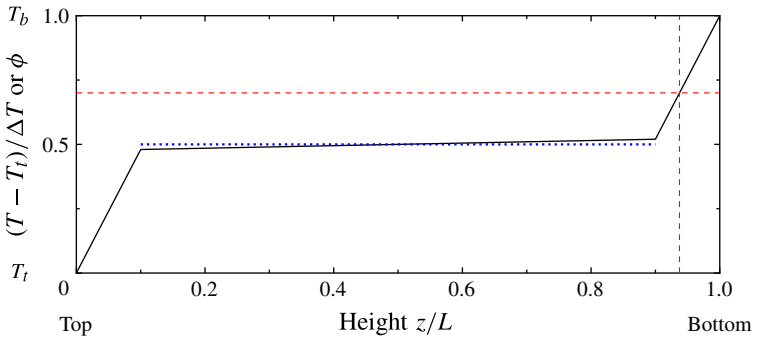

FIGURE 6. (Colour online) A schematic diagram of the vertical time-averaged temperature profile in the sample. The width of the boundary layers was increased by a factor of ten for clarity. The dotted horizontal (blue) line corresponds to T_m. The dashed horizontal (red) line represents T_{NI} for the arbitrarily chosen example $(T_{NI} - T_t)/\Delta T = 0.7$. For that case the part of the sample to the right of the vertical dashed (red) line could potentially be in the isotropic phase.

(equations (2.1)) and on the three azimuthal and temporal averages of the temperature fluctuations σ_k (equation (2.3)).

3.2.1. *Expected temperature profile*

For the interpretation of these data it is necessary to consider the typical vertical temperature profile in the sample. A schematic diagram of this profile is shown in figure 6. A lowest-order model due to Malkus (1954) assumes that half of the temperature drop ΔT occurs over each of two thermal boundary layers (BLs), one each below the top and above the bottom plate. In this approximation the sample interior, or 'bulk', is isothermal in the time average at the temperature T_m, even though its temperature may be intensely fluctuating. The thickness of the thermal BLs can then be shown to be

$$\lambda_B = L/(2Nu). \tag{3.3}$$

Looking at figure 2, one sees that the BLs are predicted to have a thickness that ranges from ∼0.7 to 1.7 per cent of the sample height. The BLs in figure 6 are shown with a width that is about a factor of ten larger for clarity. The centre temperature in the Malkus model would correspond to the dotted horizontal line. Experimental data (Lui & Xia 1998; du Puits, Resagk & Thess 2013) have shown that the Malkus temperature profiles is, for our purposes, a remarkably good first approximation although the detailed shape of the BLs is actually more intricate.

Going beyond the Malkus model, it has long been known that the bulk also sustains temperature gradients (see, e.g., Tilgner, Belmonte & Libchaber 1993; Brown & Ahlers 2007), albeit much smaller ones than those in the BLs. Although it was long thought that the gradient in the bulk was independent of z (but dependent on the radial position r), it was found recently (Ahlers *et al.* 2012) that the temperature profile actually depends logarithmically on z. However, for the present purpose we shall neglect this intricacy and focus merely on an average temperature drop across the bulk approximated by $2(T_{w,b} - T_{w,t})/\Delta T$ which, as can be seen in figure 7(*b*) below, in the single-phase region is only ∼0.04 (to be compared with approximately 0.48 for the drop across each BL in this approximation). The bulk temperature with this gradient is shown as the solid nearly horizontal line in figure 6.

3.2.2. *Single-phase regions and the onset of droplet and bubble formation*

Figure 7 presents several measured quantities as a function of T_m for $\Delta T = 6$ K. It reveals a richness of phenomena which occur as T_m is increased from low to high values (the same sequence of phenomena was observed also when T_m was decreased from high to low values). In order to discuss these in detail, we shall identify special values of T_m by introducing a second index, thus writing T_m as $T_{m,j}$, where the value of j corresponds to the corresponding value of ϕ (see (3.1) and the top horizontal axis of figure 7).

On thermodynamic grounds, a two-phase region could potentially exist from $T_{m,0} = T_{NI} - \Delta T/2 = 32.17$ °C to $T_{m,1} = T_{NI} + \Delta T/2 = 38.17$ °C. This range is indicated in the figure by the two solid vertical lines. Starting in the single-phase nematic region with $T_m < T_{m,0}$, one would expect to encounter isotropic bubble formation at the bottom plate as T_m is increased beyond $T_{m,0}$. However, no evidence of this happening is revealed by any of the measured quantities shown in the figure. The first indication of a new process, presumably the expected bubble-formation process, is found at $T_m = T_{m,on} = T_{m,0.12}$ (the left short-dashed vertical line in the figure), where the temperature in the bulk (i.e. all three $T_{w,k}$) begins to increase relative to T_m. The same onset is found also in the λ_{trans} results shown in figures 5(*b*) and 5(*d*), as discussed already in § 3.1 above. A similar, albeit smaller, delay of the onset of nematic drop formation at the top plate can be seen in $T_{w,k}$ when T_m is decreased from large values as it crosses $T_{m,1}$ (the right solid line). The onset of drop formation is indicated by the right short-dashed line and occurred at $T_{m,0.95}$. It was not resolved by the λ_{trans} data (figure 7*d*).

We note that a depression of drop formation to $T_m < T_{m,1}$ was observed also by Zhong *et al.* (2009) near the vapour pressure curve of ethane as T_m was reduced below $T_{m,1}$. Those authors were able to study this phenomenon in more detail. They found that the shift of T_m below $T_{m,1}$ for the onset of drops was independent of ΔT, i.e. it occurred at the same value $\phi = 0.95$ (in the ethane case) for all values of ΔT studied by them. However, at the low temperature end they found that the formation of bubbles at the bottom plate, although it occurred only well above $T_{m,0}$, was irreproducible from one run to another, suggesting that the bubble nucleation in their case was heterogeneous. The reproducibility, absence of hysteresis, and independence of whether T_m was increased or decreased, suggest that the nucleation process for ethane droplets (at the top plate) and for 5CB droplets or bubbles at either plate may be homogeneous.

Qualitatively one might attempt to explain the shift of the onset of bubble or droplet formation above $T_{m,0}$ or below $T_{m,1}$ respectively in terms of the temperature distribution shown in figure 6. Let us assume that $T_{m,\phi}$ barely exceeds $T_{m,0}$. Then the thickness of the layer near the bottom plate in which the phase transition could potentially occur remains very thin because the temperature gradient in the BL is steep (note that the lines in figure 6 near $z/L = 0$ and 1 are drawn with one tenth the actual slope for clarity). Thus, only a very thin layer of potentially unstable fluid exists, while a layer exceeding a minimum thickness is required for the nucleation of a droplet of critical size or larger. Roughly, one can estimate that, in the present case, the onset at $\phi = 0.12$ corresponds to a thickness of the unstable layer of $z/L \simeq 0.002$ or $z \simeq 400$ μm. However, this estimate turns out to be two orders of magnitude larger than an estimate of the critical droplet size from homogeneous nucleation theory (see, for instance, Gunton, Miguel & Sahni 1983). Thus, it appears that the simple homogeneous nucleation theory for a system in thermodynamic equilibrium is inadequate to fully explain the experimental observation of the onset shift. A possible

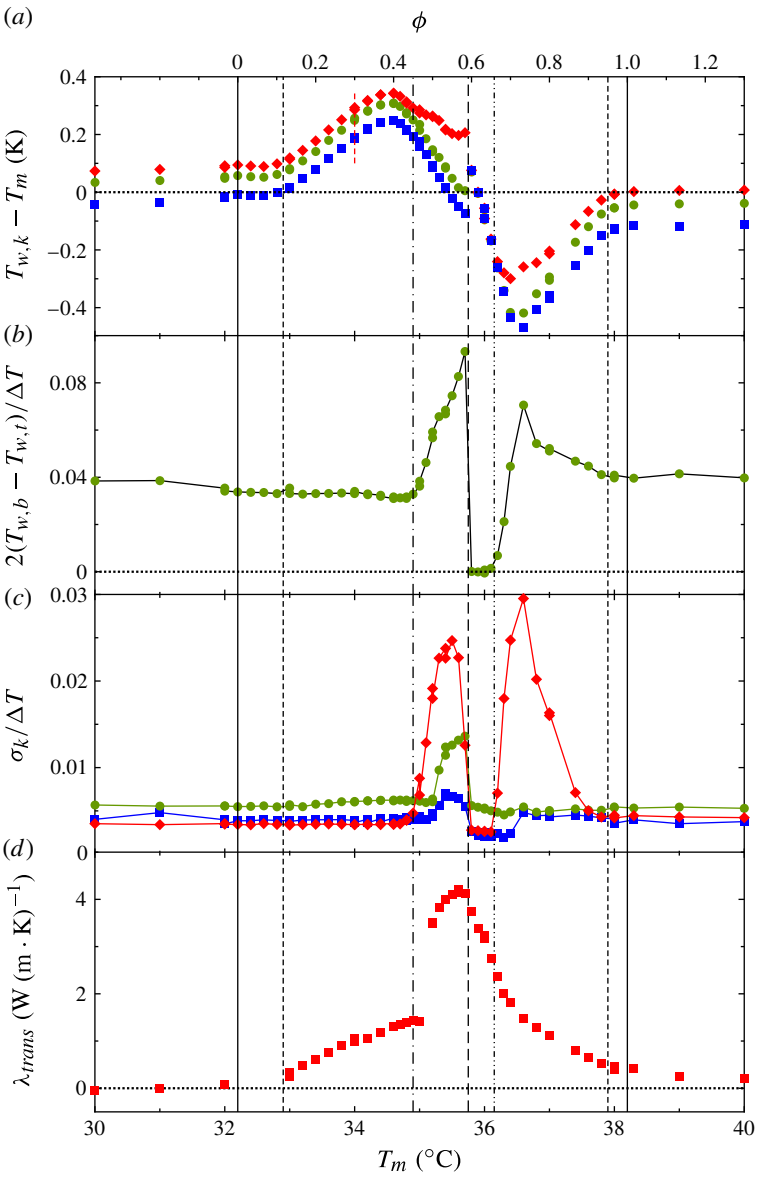

FIGURE 7. (Colour online) (*a*) Average temperature at the sidewall at heights L/4 (diamonds, red), L/2 (circles, green) and 3L/4 (squares, blue) as a function of T_m. (*b*) Temperature gradient along the sidewall, normalized by the applied temperature difference ΔT, as a function of T_m. (*c*) The azimuthal average of the root mean square deviation $\sigma/\Delta T$, obtained separately at each of the three levels and normalized by ΔT, as a function of T_m. The symbols are as in (*a*). (*d*) The excess effective conductivity λ_{trans} due to the phase transition as in figure 5(*b*). All data are time averages for $\Delta T = 6$ K. The various vertical lines separate temperature ranges that show a qualitatively different behaviour (see text for explanation). The top horizontal axis shows the temperature fraction $\phi = 0.5 + (T_m - T_{NI})/\Delta T$.

reason for this may be that the nucleation dynamics in the near-quiescent fluid deep in the interior of the BL directly adjacent to the plate is too slow, and that the turbulent

fluctuations and/or plume emissions which occur in the part of the BL which is further away from the plate are necessary to initiate droplet or bubble nucleation.

3.2.3. *Bubble formation in the bottom boundary layer*

Next we consider the system as T_m is increased further above $T_{m,0.12}$. Initially the temperature in the sample centre increases, until a maximum is reached near $T_{m,0.4}$. At constant ΔT, this implies that the heat transport across the bottom BL is enhanced relative to that across the top one and that the temperature difference across the top BL (the nature of which remains unaltered) is increased to values larger than $\Delta T/2$ in order for the two BLs to transport the same heat current. The enhanced heat transported across the bottom BL and into the bulk may be attributed to the latent heat transported by the bubbles; but it could also in part be due to a destabilization of the BL by the emission of bubbles. While the $T_{w,k}$ are increasing with T_m, our estimate of the heat current associated with the phase transition λ_{trans} also increases (see figure 7*d*). Beyond $T_{m,0.4}$ both the $T_{w,k}$ and λ_{trans} briefly decrease, until a new transition point is reached at $T_{m,0.45}$. The precise reason for the maximum and subsequent decrease is not entirely clear to us. We assume that it is associated with the approach of the isothermal plane at temperature T_{NI} to the bulk. At the transition from the BL to the bulk the profile shown in figure 6 is no longer a good approximation; the temperature profile in this region is rounded (Lui & Xia 1998; du Puits *et al.* 2013) and a more sophisticated description, for instance in terms of a Prandtl–Blasius profile (Schlichting & Gersten 2000; Prandtl 1905; Blasius 1908), would be needed but is beyond the considerations in the present paper.

It is noteworthy that both the temperature gradient in the bulk (figure 7*b*) and the fluctuations σ_k of the bulk temperatures (figure 7*c*) are essentially constant for $T_m < T_{m,0.45}$ (the dot-dashed vertical line), while the bottom BL undergoes bubble formation and the bulk temperature increases. This provides additional support to the idea that the bulk and top BL are essentially unaffected while the boiling process, including bubble formation and absorption, is restricted to the bottom BL or at least to that BL and the bottom quarter below $z = L/4$ of the bulk.

3.2.4. *Bubble penetration into the bulk*

At $T_{m,0.45}$ a new phenomenon sets in suddenly. The temperature gradient in the bulk (figure 7*b*) and the bulk temperature fluctuations (figure 7*c*) increase dramatically. Figure 7(*a*) indicates that the increase of the temperature gradient is due primarily to a slowdown of the decrease of $T_{w,b}$ (relative to $T_{w,m}$ and $T_{w,t}$), i.e. of the temperature closest to the bottom BL. Clearly at this point the boiling process is no longer restricted to the BL and the lower quarter of the bulk, but is actually penetrating into the centre of the sample. In this region we envision that the bulk continues to consist primarily of the nematic phase, but that this phase is interspersed with a high concentration of warm isotropic bubbles that originated at the bottom plate and which influence the temperature gradient and cause the vigorous temperature fluctuations displayed in figure 7(*c*).

We note that the discontinuity of λ_{trans} observed at $T_m = T_{NI} = 35.17\ ^\circ\mathrm{C}$ ($\phi = 0.5$) and displayed by the data in figure 7(*d*) is not real but instead is a consequence of the choice of λ_{exp} (see figure 5*a*) that was used to determine λ_{trans}. Ideally λ_{exp} would be the effective conductivity in the absence of latent-heat and density-discontinuity effects but in the presence of the phase transition; for a finite ΔT it would not have a sharp peak like that in figure 5(*a*) and instead would be more rounded. Unfortunately this ideal version of λ_{exp} is not known to us.

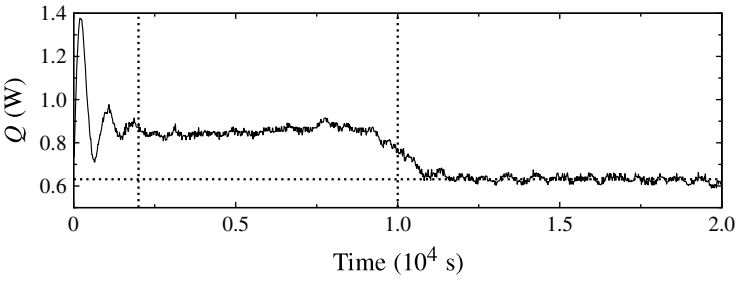

FIGURE 8. The bottom plate heater-power as a function of time for $\Delta T = 2$ K after a step of T_m from 35.4 to 35.6 °C (of ϕ from 0.615 to 0.715). The left vertical dotted line marks the time interval needed by the feedback control to reach a stable temperature difference. The right vertical dotted line indicates the approximate end of the transition to the new state. The horizontal dotted line is the average of the data over the interval from 12 000 to 20 000 s.

3.2.5. *The catastrophic inversion: the bulk becomes isotropic!*

With further increase of T_m, a catastrophic event takes place at $T_{m,0.59}$ (the longer-dashed vertical line in the figure). At this point, the temperature gradient in the bulk suddenly vanishes or becomes extremely small, and the temperature fluctuations also nearly cease to exist. We believe that an inversion takes place at $T_{m,0.59}$ where the bulk, which heretofore had consisted of the nematic phase (albeit with bubbles of isotropic fluid travelling through and being absorbed by it), is replaced by isotropic liquid. Thus, for larger T_m, only the top BL continues to consist of the nematic phase. A similar catastrophic inversion was observed also in the case of the liquid–vapour transition in ethane studied by Zhong *et al.* (2009). In that case, however, the transition was found with decreasing T_m and at $\phi = 0.43$, where the initially vapour-filled sample suddenly filled with liquid. We note that in neither case did the transition take place at the thermodynamic instability point $\phi = 1/2$, but rather at some significant interval beyond it. We assume that this shift is due to the difference between the fluid properties of the high and the low temperature phase.

Interesting support for the occurrence of the inversion comes from the time record of the experimental data. Figure 8 shows the bottom plate heater-power Q for a run with $\Delta T = 2$ K as a function of the time t. At $t = 0$ the setpoint had been changed from $T_m = 35.4$ °C (where the system had been equilibrated) to $T_m = 35.6$ °C. Initially, transients were observed due to the finite-time response of the feedback loop of the bottom plate heater. After $t \simeq 2000$ s (the left vertical dotted line in the figure), the heater power settled down, albeit not at its ultimate value. At $t = t_I \simeq 10\,000$ s, a transition took place at constant ΔT to a lower power level which was then maintained for the duration of the run (which was $\sim 8 \times 10^4$ s). Our interpretation of this phenomenon is that, for $t < t_I$, energy had to be provided to achieve the conversion of nematic to isotropic fluid. From figure 8 one can estimate the excess energy provided by considering the part of Q above the horizontal dotted line for $t < 10\,000$ s. After subtracting contributions needed to heat the sample and its container, we find this estimate to be $\sim$1.7 kJ. Given a latent heat of 1.56 kJ kg^{-1} (Thoen 1992; van Roie *et al.* 2005), this energy is enough to convert $\sim$1.1 kg of 5CB from the nematic to the isotropic phase. Our actual sample mass was 1.4 kg, not very different from the above semi-quantitative estimate. Similar results were obtained also with $\Delta T = 1$ and 6 K. When the experiment was conducted by decreasing T_m from 35.6 to 35.4 °C, the bottom plate heater-power settled down on its final value immediately after the

initial transients which were restricted approximately to the first 2000 s. This can be understood since the heat generated by the isotropic-to-nematic transition throughout the bulk is dissipated at the top plate which would lead to an increased cooling necessary to maintain the top plate temperature. This quantity, however, was not measured in the experiment.

3.2.6. *An interval of 'superconductivity'*

Returning our attention to figure 7, we note that there is a short interval of T_m beyond $T_{m,0.59}$, up to $T_{m,0.66}$, over which the thermal gradient in the bulk vanishes within our resolution (see figure 7*b*) and where the temperature fluctuations σ_k (see figure 7*c*) become smaller than they were in the single-phase nematic or isotropic fluid ($\phi < 0$ or $\phi > 1$). Also noteworthy is that over this interval the bulk temperature $T_{w,k}$ decreased significantly, as seen in figure 7(*a*). We do not really have a good explanation for the existence of this interval of essentially vanishing thermal gradients and fluctuation amplitudes. It seems as if bubbles (droplets) are forming in the upper (lower) part of the bottom (top) boundary layer or even in the lower (upper) part of the bulk. These bubbles (droplets) have a temperature very close to the bulk temperature and are thus not visible in the σ_k measurements. However, the exact processes in this range are unknown to us, and it would be of interest to investigate this state further by local temperature measurements in the sample interior.

3.2.7. *Droplet formation in the top boundary layer*

Beyond $T_{m,0.66}$ the observed phenomena are essentially the reverse of what was seen from $T_{m,1}$ to $T_{m,0.59}$ and described in §§ 3.2.2 and 3.2.3, albeit over a somewhat smaller interval of T_m. The data for $T_{w,k}$ and σ_k suggest that from $T_{m,0.66}$ to $T_{m,0.96}$ nematic droplet formation continued in the top BL, while finally for $T_m > T_{m,0.96}$ the entire sample was isotropic.

4. Summary and conclusion

We used the nematic liquid crystal 4-Cyano-4′-pentylbiphenyl (5CB) to study thermal convection while a *soft* phase transition from the nematic to the isotropic state or *vice versa* (the 'clearing point' at a temperature $T_{NI} = 35.17$ °C) was present in the sample. This problem is of fundamental interest for its own sake, but is also relevant to the geophysical phenomenon of convection in the Earth's mantle where several phase transitions with small latent heats ΔH and small density discontinuities take place at various depths (see, for instance, Christensen 1995).

We covered with our data Rayleigh numbers in the range $3 \times 10^7 \leqslant Ra \leqslant 6 \times 10^8$, which is similar to that of mantle convection. Whereas in the mantle the Prandtl number is effectively infinite, many features of thermally driven convection do not change very much above $Pr \simeq 400$ (see, for instance, Ahlers *et al.* 2009) which is typical of 5CB. The latent heat at the clearing point is 1.57 kJ kg^{-1} (Thoen 1992; van Roie *et al.* 2005), which is not very different from the range 0.4 to 1.2 kJ kg^{-1} relevant to the geological cases (Verhoogen 1965). The density discontinuity of 5CB at T_{NI} is, however, an order of magnitude smaller than it is for the geophysical system. Beyond these comparisons there are of course many differences between the enormously complex geophysical problem and the highly idealized laboratory experiment.

In § 3.1 we presented measurements of the effective thermal conductivity λ_{eff} of the 5CB sample both well above and well below T_{NI} in the single-phase regions, as well as closer to T_{NI} where the applied temperature difference straddled the transition

temperature. In the single-phase regions the corresponding Nusselt number Nu agreed with measurements for isotropic fluids (Weiss & Ahlers 2013), but in the two-phase region there was a significant additional contribution to λ_{eff} which we attribute to latent heat carried by bubbles of isotropic fluid generated in the bottom or droplets of nematic fluid generated in the top boundary layer. Due to the small value of ΔH, the enhancement of λ_{eff} never exceeded a factor of two or so. This can be compared with the enhancement by an order of magnitude in the case of ethane near its vapour pressure curve (Zhong *et al.* 2009) where ΔH varies from $\sim$500 kJ kg^{-1} at the normal boiling point to zero at the critical point.

In § 3.2 we elucidated the processes of nematic droplet and isotropic bubble formation at the cold (top) and hot (bottom) end of the sample respectively where the system sustains thermal boundary layers (BLs). For our system these BLs had a thickness of about a mm each, which is thin compared to the sample height (see § 3.2.1). Each of the BLs sustained nearly half of the temperature drop across the entire system, leaving the bulk nearly isothermal. The measurements consisted of the temperatures along the sidewall of the sample and of the time evolution of the heat current needed to maintain a prescribed temperature. This was done in greatest detail for an applied temperature difference of $\Delta T = 6$ K. A complex sequence of events took place as the mean temperature T_m of the sample was increased from values in the single-phase region well below T_{NI} to much higher values well above T_{NI} (an equivalent sequence of events was seen when T_m was reduced from larger values). We shall discuss them in terms of the temperature fraction $\phi = 0.5 + (T_m - T_{NI})/\Delta T$. Note that $\phi = 0$ when $T_b = T_{NI}$, and $\phi = 1$ when $T_t = T_{NI}$. The observed events can be summarized as follows.

(i) When the bottom temperature T_b of the sample passed T_{NI} ($\phi = 0$) so that thermodynamically the formation of isotropic 5CB in the bottom boundary layer became possible, the system remained nematic until a 'superheating' ($T_b > T_{NI}$) by $\sim 0.12\Delta T$ ($\phi = 0.12$) was achieved (see § 3.2.2). At that level of superheating we estimate that the thickness of the fluid layer in the bottom boundary with $T > T_{NI}$ was $\sim$400 μm, which is much thicker than simple estimates of the critical bubble size for homogeneous nucleation (see, for instance, Gunton *et al.* 1983). The phenomenon is similar to what was observed for ethane near its vapour pressure curve by Zhong *et al.* (2009). While it remains unexplained in detail, we conjecture that turbulent fluctuations of the supersaturated fluid are necessary to initiate bubble formation and/or growth at a significant rate, and that the fluid in the BL but immediately adjacent to the plate does not sustain fluctuations of sufficient size to promote this process.

(ii) As ϕ was increased beyond 0.12, the contribution λ_{trans} from the latent heat to the heat transport became noticeable and the temperature in the bulk began to increase while temperature gradients and fluctuations in the bulk remained unaffected (see § 3.2.3). We take this to mean that bubble formation near the bottom plate had started but that the bubbles were still confined to the bottom BL.

(iii) As ϕ increased beyond 0.44, the temperature gradient and fluctuations in the bulk increased, indicating that bubble formation, initiated in the bottom BL, was penetrating the bulk (see § 3.2.4).

(iv) When ϕ reached 0.59, a catastrophic inversion took place where the nematic fluid in the bulk was suddenly replaced by isotropic fluid (see § 3.2.5). This event was reflected in the time evolution of the bottom plate power needed to provide the

latent heat of about 1 kJ and to maintain the system at a constant ΔT while the inversion was taking place.

(v) The inversion was followed by a remarkable interval of ϕ, up to $\phi = 0.66$, over which the temperature gradient in the bulk vanished within our resolution and the fluctuation amplitudes became even smaller than they were in the single-phase regions (see § 3.2.6). We do not have a good explanation for this remarkable 'superconducting' state.

(vi) For the remainder of the run, up to $\phi > 1$, the sequence of events was the reverse of what had happened up to $\phi = 0.59$, except that it took place near and in the top BL where nematic droplets were now forming in a generally isotropic sample. The droplet formation was not a precise mirror image of the bubble formation; we attribute this to the differing physical properties of the isotropic and nematic phases.

Acknowledgement

This work was supported by the US National Science Foundation through grant DMR11-58514.

REFERENCES

AHLERS, G. 1995 *Experiments on Thermally Driven Convection*. Springer.

AHLERS, G. 2009 Turbulent convection. *Physics* **2**, 74.

AHLERS, G., BERGE, L. & CANNELL, D. 1993 Thermal convection in the presence of a first-order phase change. *Phys. Rev. Lett.* **70**, 2399–2402.

AHLERS, G., BODENSCHATZ, E., FUNFSCHILLING, D., GROSSMANN, S., HE, X., LOHSE, D., STEVENS, R. & VERZICCO, R. 2012 Logarithmic temperature profiles in turbulent Rayleigh–Bénard convection. *Phys. Rev. Lett.* **109**, 114501.

AHLERS, G., BROWN, E., FONTENELE ARAUJO, F., FUNFSCHILLING, D., GROSSMANN, S. & LOHSE, D. 2006 Non-Oberbeck–Boussinesq effects in strongly turbulent Rayleigh–Bénard convection. *J. Fluid Mech.* **569**, 409–445.

AHLERS, G., CALZAVARINI, E., FONTENELE ARAUJO, F., FUNFSCHILLING, D., GROSSMANN, S., LOHSE, D. & SUGIYAMA, K. 2008 Non-Oberbeck-Boussinesq effects in turbulent thermal convection in ethane close to the critical point. *Phys. Rev.* E **77**, 046302.

AHLERS, G., CANNELL, D. S., BERGE, L. I. & SAKURAI, S. 1994 Thermal conductivity of the nematic liquid crystal 4-*n*-pentyl-4′-cyanobiphenyl. *Phys. Rev.* E **49**, 545–553.

AHLERS, G., FONTENELE ARAUJO, F., FUNFSCHILLING, D., GROSSMANN, S. & LOHSE, D. 2007 Non-Oberbeck–Boussinesq effects in gaseous Rayleigh–Bénard convection. *Phys. Rev. Lett.* **98**, 054501.

AHLERS, G., GROSSMANN, S. & LOHSE, D. 2009 Heat transfer and large scale dynamics in turbulent Rayleigh-Bénard convection. *Rev. Mod. Phys.* **81**, 503–538.

AUERNHAMMER, G., VOLLMER, D. & VOLLMER, J. 2005 Oscillatory instabilities in phase separation of binary mixtures: fixing the thermodynamic driving. *J. Chem. Phys.* **123** (13), 134511.

BEZRODNA, T., CHASHECHNIKOVA, I., GAVRILKO, T., PUCHKOVSKA, G., SHAYDYUK, Y., TOLOCHKO, A., BARAN, J. & DROZD, M. 2008 Structure formation and its influence on thermodynamic and optical properties of montmorillonite organoclay-5CB liquid crystal nanocomposites. *Liquid Cryst.* **35**, 265–274.

BLASIUS, H. 1908 Grenzschichten in Flüssigkeiten mit kleiner Reibung. *Z. Math. Phys.* **56**, 1–37.

BOUSSINESQ, J. 1903 *Theorie Analytique de la Chaleur*, vol. 2, Gauthier-Villars.

BRENT, A. D., VOLLER, V. R. & REID, K. J. 1988 Enthalpy–porosity technique for modelling convection–diffusion phase change: application to the melting of a pure metal. *Numer. Heat Transfer* **13**, 297–318.

BROWN, E. & AHLERS, G. 2007 Temperature gradients, and search for non-Boussinesq effects, in the interior of turbulent Rayleigh-Bénard convection. *Europhys. Lett.* **80**, 14001.

BROWN, E., NIKOLAENKO, A. & AHLERS, G. 2005 Reorientation of the large scale circulation in turbulent Rayleigh–Bénard convection. *Phys. Rev. Lett.* **95**, 084503.

BUSSE, F. H. & SCHUBERT, G. 1971 Convection in a fluid with two phases. *J. Fluid Mech.* **46** (4), 801–812.

CHILLÀ, F. & SCHUMACHER, J. 2012 New perspectives in turbulent Rayleigh–Bénard convection. *Eur. Phys. J.* E **35**, 58.

CHRISTENSEN, U. 1995 Effects of phase transitions on mantle convection. *Annu. Rev. Earth Planet. Sci.* **23**, 65–87.

DHIR, V. K. 1998 Boiling heat transfer. *Annu. Rev. Fluid Mech.* **30**, 365–401.

FUNFSCHILLING, D., BROWN, E. & AHLERS, G. 2008 Torsional oscillations of the large scale circulation in turbulent Rayleigh–Bénard convection. *J. Fluid Mech.* **607**, 119–139.

DE GENNES, P. & PROST, J. 1995 *The Physics of Liquid Crystals*. Oxford University Press.

GUNTON, J. D., MIGUEL, M. S. & SAHNI, P. S. 1983 The dynamics of first-order phase transitions. In *Phase Transitions and Critical Phenomena* (ed. C. Domb & J. L. Lebowitz), p. 267. Academic Press.

HARTMANN, D. L., MOY, L. A. & FU, Q. 2001 Tropical convection and the energy balance at the top of the atmosphere. *J. Clim.* **14**, 4495–4511.

IEZZI, R., FRANCOLINO, S. & MUCCHETTI, G. 2011 Natural convective cooling of cheese: predictive model and validation of heat exchange simulation. *J. Food Engng* **106** (1), 88–94.

JACOBS, M. H. & VAN DEN BERG, A. P. 2011 Complex phase distribution and seismic velocity structure of the transition zone: convection model predictions for a magnesium-endmember olivine–pyroxene mantle. *Phys. Earth Planet. Inter.* **186** (1/2), 36–48.

KADANOFF, L. P. 2001 Turbulent heat flow: structures and scaling. *Phys. Today* **54** (8), 34–39.

KERR, R. 1992 Having it both ways in the mantle. *Science* **258** (5088), 1576–1578.

KHOO, I.-C. 2007 *Liquid Crystals*. Wiley.

KRAMER, L. & PESCH, W. 1995 Convection instabilities in nematic liquid crystals. *Annu. Rev. Fluid Mech.* **27**, 515–539.

KÜHN, M., BOSBACH, J. & WAGNER, C. 2009 Experimental parametric study of forced and mixed convection in a passenger aircraft cabin mock-up. *Build. Environ.* **44** (5), 961–970.

LOHSE, D. & XIA, K.-Q. 2010 Small-scale properties of turbulent Rayleigh–Bénard convection. *Annu. Rev. Fluid Mech.* **42**, 335–364.

LUI, S. L. & XIA, K.-Q. 1998 Spatial structure of the thermal boundary layer in turbulent convection. *Phys. Rev.* E **57**, 5494–5503.

MALKUS, M. V. R. 1954 The heat transport and spectrum of thermal turbulence. *Proc. R. Soc. Lond.* A **225**, 196–212.

MARSHALL, J. & SCHOTT, F. 1999 Open-ocean convection: observations, theory, and models. *Rev. Geophys.* **37**, 1–64.

OBERBECK, A. 1879 Über die Wärmeleitung der Flüssigkeiten bei Berücksichtigung der Strömungen infolge von Temperaturdifferenzen. *Ann. Phys. Chem.* **7**, 271–292.

PAULUIS, O. & SCHUMACHER, J. 2011 Self-aggregation of clouds in conditionally unstable moist convection. *Proc. Natl. Acad. Sci. USA* **108**, 12623–12628.

PRANDTL, L. 1905 *Über Flüssigkeitsbewegung bei sehr kleiner Reibung*, pp. 484–491 Teubner.

DU PUITS, R., RESAGK, C. & THESS, A. 2013 Thermal boundary layers in turbulent Rayleigh–Bénard convection at aspect ratios between 1 and 9. *New J. Phys.* **15**, 013040.

RAHMSTORF, S. 2000 The thermohaline ocean circulation: a system with dangerous thresholds? *Climate Change* **46**, 247–256.

VAN ROIE, B., LEYS, J., DENOLF, K., GLORIEUX, C., PITSI, G. & THOEN, J. 2005 Weakly first-order character of the nematic–isotropic phase transition in liquid crystals. *Phys. Rev.* E **72**, 041702–1–8.

SAKURAI, S., TSCHAMMER, A., PESCH, W. & AHLERS, G. 1999 Convection in the presence of a first-order phase change. *Phys. Rev.* E **60**, 539–550.

SCHLICHTING, H. & GERSTEN, K. 2000 *Boundary Layer Theory*, 8th edn. Springer.

SCHUBERT, G. 1992 Numerical models of mantle convection. *Annu. Rev. Fluid Mech.* **24**, 359–394.

SHIM, S., DUFFY, T. & SHEN, G. 2001 The post-spinel transformation in Mg_2SIO_4 and its relation to the 660 km discontinuity. *Nature* **411**, 571–574.

STEVENS, B. 2005 Atmospheric moist convection. *Annu. Rev. Earth Planet. Sci.* **33**, 605–643.

THOEN, J. 1992 Calorimetric studies of liquid crystal phase transitions: steady state adiabatic techniques. In *Phase Transition in Liquid Crystals*. Plenum.

TILGNER, A., BELMONTE, A. & LIBCHABER, A. 1993 Temperature and velocity profiles of turbulence convection in water. *Phys. Rev.* E **47**, R2253–R2256.

TONG, L. & TANG, Y. 1997 *Boiling Heat Transfer and Two-Phase Flow*. Taylor & Francis.

VERHOOGEN, J. 1965 Phase changes and convection in the earth's mantle. *Phil. Trans. R. Soc. Lond.* A **258** (1088), 276–283.

WEIDAUER, T., PAULUIS, O. & SCHUMACHER, J. 2010 Cloud patterns and mixing properties in shallow moist Rayleigh–Bénard convection. *New J. Phys.* **12**, 105002.

WEINSTEIN, S. A. 1993 Catastrophic overturn of the mantle driven by multiple phase changes and internal heat generation. *Geophys. Res. Lett.* **20**, 101.

WEISS, S. & AHLERS, G. 2011 Turbulent Rayleigh–Bénard convection in a cylindrical container with aspect ratio $\Gamma = 0.50$ and Prandtl number $Pr = 4.38$. *J. Fluid Mech.* **676**, 5–40.

WEISS, S. & AHLERS, G. 2013 Magnetic-field effect on turbulent thermal convection of a nematic liquid crystal. *J. Fluid Mech.* **716**, R7.

ZERBAN, A. H. & NYE, E. P. 1956 *Power Plants*, 2nd edn. International Textbook Company.

ZHONG, J.-Q., FUNFSCHILLING, D. & AHLERS, G. 2009 Enhanced heat transport by turbulent two-phase Rayleigh–Bénard convection. *Phys. Rev. Lett.* **102**, 124501.